The Journal of Physical Chemistry B

 VOLUME 102, NUMBER 45, NOVEMBER 5, 1998

LETTERS

High-Resolution Structural Study of an Electrical Double Layer by Neutron Diffraction

Graham D. Williams,*,† Alan K. Soper,‡ Neal T. Skipper,† and Martin V. Smalley†

Department of Physics and Astronomy, University College London, Gower Street, London WC1E 6BT, U.K., and ISIS Neutron Division, Rutherford Appleton Laboratory, Chilton, Didcot, Oxfordshire OX11 0QX, U.K.

Received: July 15, 1998; In Final Form: September 1, 1998

We present the first high-resolution study of the aqueous structure developed in the electrical double layer region of a colloidal clay system. Our samples were highly oriented vermiculite gels containing isotopically labelled propylammonium counterions: $C_3\mathbf{H}_7NH_3^+$ and $C_3\mathbf{D}_7NH_3^+$. The gels were prepared with a clay layer spacing of 43.6 Å. Time-of-flight neutron diffraction was used to measure the scattering intensity normal to the clay surfaces, from which the neutron scattering density was refined by an inverse Monte Carlo method. Diffraction data from two isotopically distinct samples were fitted simultaneously, thereby allowing us to locate the labelled propyl groups unambiguously. Our results show that the counterions in our vermiculite gels are separated from the clay surfaces by two layers of partially ordered water molecules. In fact, the counterion density reaches a maximum at the center of the interlayer region. The measured structure is therefore at odds with traditional primitive models of the electrical double layer. Such models place the maximum of the counterion density adjacent to the vermiculite clay surfaces, in the so-called Stern layer.

Introduction

A detailed knowledge of the structure developed in the electrical double layer (EDL)[1] is essential for understanding many important processes, including colloidal interactions, electrode reactions, crystal growth and dissolution, polypeptide folding, and membrane formation.[2,3] Unfortunately, in most real systems the surface area presented to the liquid is relatively small and/or poorly oriented. High-resolution structural studies of the electrical double layer region are therefore extremely difficult.[4] Vermiculite clays are a notable exception.

Vermiculites are expandable clay minerals that occur naturally as macroscopic crystals, typically mm^3-cm^3 in volume. Such crystals consist of a stack of $\sim 10^6$ negatively charged mica-like sheets, held together by charge-balancing interlayer counterions.[5] These interlayer counterions are exchangeable and can be selected by soaking the vermiculite crystals in an appropriate solution. In the presence of water or aqueous solutions the interlayer counterions have a tendency to hydrate, thereby forcing the clay layers apart. Typically this expansion is limited to a few molecular layers of water and is known as crystalline swelling. However, with certain interlayer counterions, notably propylammonium ($C_3H_7NH_3^+$) and butylammonium ($C_4H_9NH_3^+$),[6] very large volumes of water can be absorbed between the clay layers. These macroscopically swollen vermiculite crystals form a highly oriented gel phase, with a regular clay layer spacing, d, of up to $\sim$600 Å.[7,8]

Alkylammonium vermiculite gels undergo a reversible phase transition to the crystalline state, above about 14 °C.[7] This entropically driven collapse is probably caused by hydrophobic hydration of the counterions. However, below the phase transition temperature, the gels behave as ideal one-dimensional colloids: the separation of the clay layers is inversely proportional to the square root of the ionic strength.[7,8] This relationship is predicted by primitive model theories,[9−11] and is observed experimentally in smectite clays containing sodium[12] and

† University College London.
‡ Rutherford Appleton Laboratory.

10.1021/jp983034q CCC: $15.00
Published on Web 10/16/1998

TABLE 1: Coherent Neutron Scattering Lengths, *b*, of Selected Atomic Species

species	*b*/fm	species	*b*/fm
H	−3.741	Al	3.449
D	6.671	Mg	5.375
O	5.803	C	6.646
Si	4.149	N	9.36

lithium[13] counterions. Alkylammonium vermiculite gels are therefore superb systems with which to study the EDL and colloidal interactions and thereby test the assumptions and predictions of theoretical models.

We have exploited time-of-flight (ToF) neutron diffraction to study the aqueous structure in propylammonium vermiculite gels, prepared with a clay layer spacing of 43.6 Å. This choice of technique has decisive advantages. First, we are able to use isotopic labelling of $C_3\mathbf{D}_7NH_3^+$ for $C_3\mathbf{H}_7NH_3^+$, in conjunction with difference analysis, to locate the interlayer counterions and water molecules unambiguously: both hydrogen (H) and deuterium (D) scatter neutrons strongly, but their scattering lengths have opposite signs (Table 1). Second, we are able to exploit the extremely large range of scattering vectors, *Q*, which can be measured in a single ToF neutron diffraction experiment. Our data therefore provide a uniquely detailed picture of both the long-range and short-range structure.

Experimental Methods

The vermiculite used in the experiments comes from Eucatex, Brazil, and has the formula[14]

$$[Si_{3.07}\,Mg_{2.72}\,Al_{0.83}\,Fe_{0.25}\,Ti_{0.06}\,Ca_{0.06}\,Cr_{0.005}\,K_{0.005}\,O_{10}(OH)_2]M^+_{0.65}\cdot nH_2O$$

where the species in square brackets represent the composition of the clay layers. Eucatex vermiculite occurs naturally as flakes of ∼5 mm × 5 mm × 1 mm. These flakes were soaked for 1 year in a 1 M (aq) NaCl solution in order to remove the naturally occurring counterions. The resulting sodium Eucatex was then exchanged in a 1 M (aq) $C_3H_7NH_3Cl$ solution to give propylammonium ($PrNH_3$) Eucatex. Twenty flakes of $PrNH_3$ Eucatex were placed in a 0.5 M solution of $C_3H_7NH_3Cl$ in D_2O and left to swell for 5 days.

Experiments were conducted on the LAD time-of-flight diffractometer[15] at the ISIS pulsed neutron source, Rutherford Appleton Laboratory, U.K.[15] Samples were contained in a flat-plate can made from a null coherent scattering Ti/Zr alloy. The sample container was mounted on a rotating closed cycle refrigerator, and the temperature was maintained at 4 °C. Isotopic labelling of the counterions was conducted in situ, by replacing $C_3\mathbf{H}_7ND_3^+$ with $C_3\mathbf{D}_7ND_3^+$ in the swelling solution. The samples were aligned with respect to the neutron beam and a chosen detector bank so that the *c** axis of the gel was parallel to the scattering vector, **Q**.[15] With this orientation the measured coherent neutron scattering intensity, *I*(*Q*), consists of the (00*l*) Bragg reflections.

The LAD diffractometer uses neutrons with wavelengths of 0.1−6 Å. It has 14 detector banks arranged around the sample, at scattering angles of between 5° and 150° in 2θ. During our current experiments, two separate runs were conducted for each sample, corresponding to scattering into the detector banks at 5° and 35°. By joining these two data sets, we achieve a total scattering vector range of 0.1 Å^{-1} < *Q* < 12 Å^{-1}. The lower limit allows us to measure the intensity of the (001) Bragg reflection, while the upper limit provides us with real space resolution of 0.5 Å.

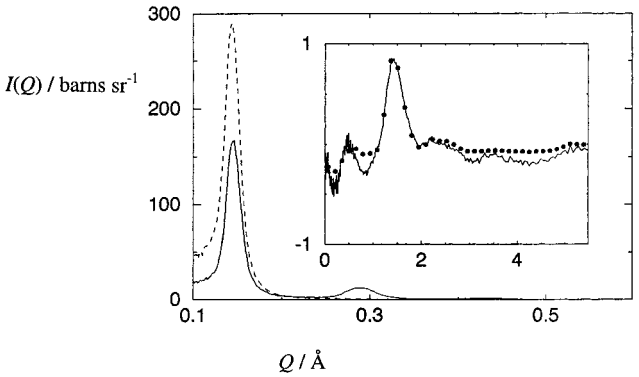

Figure 1. Neutron scattering intensity, *I*(*Q*) (eq 1), for 43.6 Å propylammonium vermiculite gels. Data are presented as a function of counterion isotope: dotted line, $C_3\mathbf{H}_7ND_3^+$; solid line, $C_3\mathbf{D}_7ND_3^+$. The main figure illustrates how isotope substitution creates a large difference in the (001) and (002) Bragg peak intensities. The (003) peak was also individually resolved but cannot be seen in this figure owing to scale limitations. The inset shows the data for the $C_3\mathbf{D}_7ND_3^+$ sample (solid line), illustrating how the Bragg peaks are not individually resolved at higher *Q*. The inset also shows the calculated peak intensities for the $C_3\mathbf{D}_7ND_3^+$ sample (circles), illustrating that the fitted profiles shown in Figure 2 are consistent with the experimental data.

The raw data were corrected for absorption and multiple scattering, and for scattering due to the background, sample container, and soaking solution. Corrected data were put on an absolute scale by reference to the known scattering from a vanadium rod. The normalized coherent neutron scattering intensities are presented as a function of counterion isotope in Figure 1. The (001) to (003) peaks are clearly visible, and their positions show that both samples have a regular clay layer separation of 43.6 Å. At higher *Q*-values the Bragg peaks are not individually resolved but combine to give rise to broader features.

The normalized neutron scattering intensities, *I*(*Q*), are related to the neutron scattering density profiles normal to the clay sheets, $\rho(z)$, via the crystallographic structure factor, *S*(*Q*)

$$I(Q) = M(Q)\,S(Q)\,S^*(Q) \qquad (1)$$

$$S(Q) = \int_0^c \rho(z)[\cos(Qz) + i\,\sin(Qz)]\,dz \qquad (2)$$

where *c* is the clay layer spacing, *z* is the position on the clay *c**-axis, and *M*(*Q*) is a Lorentzian that takes into account the mosaic spread of the sample.[16] This essentially crystallographic description is a novel treatment that is valid along the *c**-axis. It encompasses the periodically repeated liquid layers present in our gels and has the advantage that it produces a single-particle distribution function, $\rho(z)$, rather than a spatially averaged pair distribution function. We are therefore able to locate the water molecules and counterions unambiguously, with respect to their distance from the clay surfaces.

Neutron scattering density profiles were obtained simultaneously for both isotopic compositions using an inverse Monte Carlo refinement,[16] as follows. Two arrays were set up, $\rho(z)_1$ and $\rho(z)_2$, each containing 150 moveable "particles". Every particle is associated with a Gaussian distribution of neutron scattering intensity. The two arrays were combined to produce scattering density profiles representing the hydrogenated and deuterated samples, $\rho(z)_H$ and $\rho(z)_D$

$$\rho(z)_H = \rho(z)_1 + b_H\rho(z)_2 \qquad \rho(z)_D = \rho(z)_1 + b_D\rho(z)_2$$

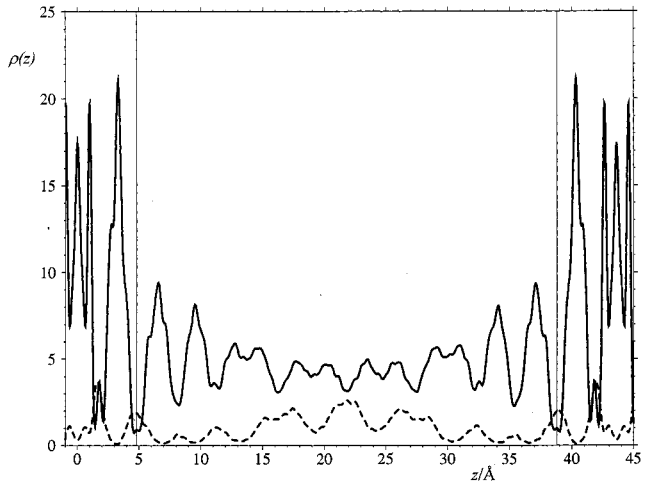

Figure 2. Neutron scattering density profiles normal to the clay layers, $\rho(z)$ (eq 2), for 43.6 Å propylammonium substituted vermiculite gels. To highlight the contrast arising from isotopic substitution, we present two profiles. The solid line shows the contribution from all species that are not isotopically labelled. The dashed line shows the contribution from the substituted alkyl hydrogen atoms, plus ongoing exchange of H/D in the clay layers. This profile has been expanded by 100% along the $\rho(z)$ axis. The lines at $z = 4.8$ Å and $z = 38.8$ Å indicate the van der Waals surfaces of the clay layers. The common profile has peaks at 6.6 and 9.6 Å (and 37.0 and 34.0 Å) indicating that there are two layers of water molecules associated with each surface. The difference profile shows that the majority of the counterions are broadly distributed around the midplane of the interlayer region.

where b_H and b_D are the scattering lengths of hydrogen and deuterium, respectively (Table 1). The density profile $\rho(z)_2$ then gives the location of the substituted alkyl protons: the "difference profile". The profile $\rho(z)_1$ gives the location of all atoms common to both samples (clay layers, water molecules, and the unlabelled portion of the counterions): the "common profile".

The starting configuration for the refinement was the clay layer structure derived from X-ray diffraction and chemical analysis.[5] All other particles were distributed evenly over the system. The positions of all particles, including those in the clay layer, were then sampled by an inverse Monte Carlo routine. This weights acceptance of particle moves by comparing the experimental $I(Q)$ with the one calculated from the model profiles, $\rho(z)_H$ and $\rho(z)_D$, using eqs 1 and 2. The final profiles, averaged over 100 000 equilibrated configurations, are presented in Figure 2. The average R-factors for the final fits were <1% (Figure 1, inset).

Results and Discussion

The fitted common and difference scattering density profiles for $C_3(\mathbf{H/D})_7ND_3$ vermiculite are shown in Figure 2. In the common profile, sharp peaks in the regions 0.0−3.3 and 40.3−43.6 Å are due to the atoms in the crystalline clay layers. The positions and areas of these peaks are in excellent agreement with X-ray data and chemical analysis (Table 2).

Moving into the interlayer region, we observe strong common peaks at 6.6 and 9.6 Å (and 37.0 and 34.0 Å). A much weaker pair of peaks is also seen at 12.6 and 31.0 Å. The difference profile has a broad peak across the interlayer region. This has a maximum scattering density around the midplane (at $z = 21.8$ Å) and an oscillatory component giving rise to smaller maxima at 11.2 and 32.4 Å. Two pairs of smaller peaks are also observed in the clay layer region of the difference profile at 1.7 (41.9) and 4.7 Å (38.9 Å). The areas of these peaks are listed in Table 2.

TABLE 2: Analysis of Peak Areas in the Fitted Density Profiles for 43.6 Å $PrNH_3$ Vermiculite Gels, Showing the Limits of Integration (Å), the Assignment of Chemical Species to Each Peak, Which Profile the Peak Occurs in, the Peak Area (10^{-14} m), and the Number of Atoms Corresponding to These Areas[a]

position	assignment	profile	area	chemical equivalent
0.0−0.64	O_h cations	common	1.58	O_h cations, 0.79 excess
0.64−1.46	O (clay)	common	1.75	3 O
1.46−2.1	D (clay)	common	0.384	0.6 D
2.1−4.8	T_h cations, O (clay), H_2O	common	5.24	T_h cations, 3O, 1.4D_2O
0.9−3.3	H/D (clay)	difference	0.35	0.6 H/D
4.8−8.1	D_2O	common	3.7	1.93 D_2O
3.3−6.7	H/D (D_2O)	difference	0.33	0.6 H/D
8.1−11.1	D_2O	common	3.5	1.81 D_2O
11.1−32.5	D_2O, C_3-ND_3	common	21.2	0.65 C_3-ND_3, 9.5 D_2O
13.4−30.2	H/D (alkyl)	difference	1.06	0.61 H_7

[a] The number of atoms assigned to the fitted profiles is in good agreement with the known composition of the clay unit cell, except for the peak due to the octahedral cations in the clay layer, where roughly twice the expected scattering intensity is seen in the fitted profile.

We conclude from the main peak in the difference profile that the majority of the alkyl groups of the counterions are broadly located around the center of the interlayer region. This is consistent with the slight dip observed across the center of the common profile, arising from the partial exclusion of D_2O molecules by the counterions. It should be noted, however, that the partial volume of the counterions[17] is only ∼15% of the total volume of the region over which they are spread. There is therefore no evidence to suggest significant aggregation of the hydrophobic propyl groups.

Having established that the majority of the counterions are located around the center of the interlayer, we attribute the peaks at 6.6 and 9.6 Å (37.0 and 34.0 Å) in the common profile to two layers of water molecules associated with each clay surface. The position of the third pair of peaks in the common profile is consistent with a less well-defined third layer formed either by water molecules or by the ND_3^+ headgroups of the counterions. The peaks at 11.2 and 32.4 Å in the difference profile suggest that a small proportion of the ND_3^+ headgroups are also incorporated into the second layer of water molecules, giving an oscillatory component to the counterion distribution. Figure 3 shows a molecular graphics snapshot of the system, illustrating the two layers of partially orientated water molecules and the maximum counterion density at the center of the interlayer region. It should be noted, however, that this single snapshot, containing only 12 propylammonium counterions, cannot reproduce all the features of the averaged scattering density profiles.

The peaks in the clay layer region of the difference profile are attributed to ongoing replacement of hydrogen in the clay layers by deuterium during the 4 days between collection of data from the three samples. The peaks at 1.7 Å (41.9 Å) are consistent with exchange of protons on hydroxyl groups in the clay layer, while the peaks at 4.9 Å (38.9 Å) are consistent with exchange of protons on water molecules strongly adsorbed to the hexagonal cavities of the clay surface. While no data are available on exchange rates in propylammonium vermiculite, the time scale involved would be comparable with rates observed in other mica-like minerals.[18]

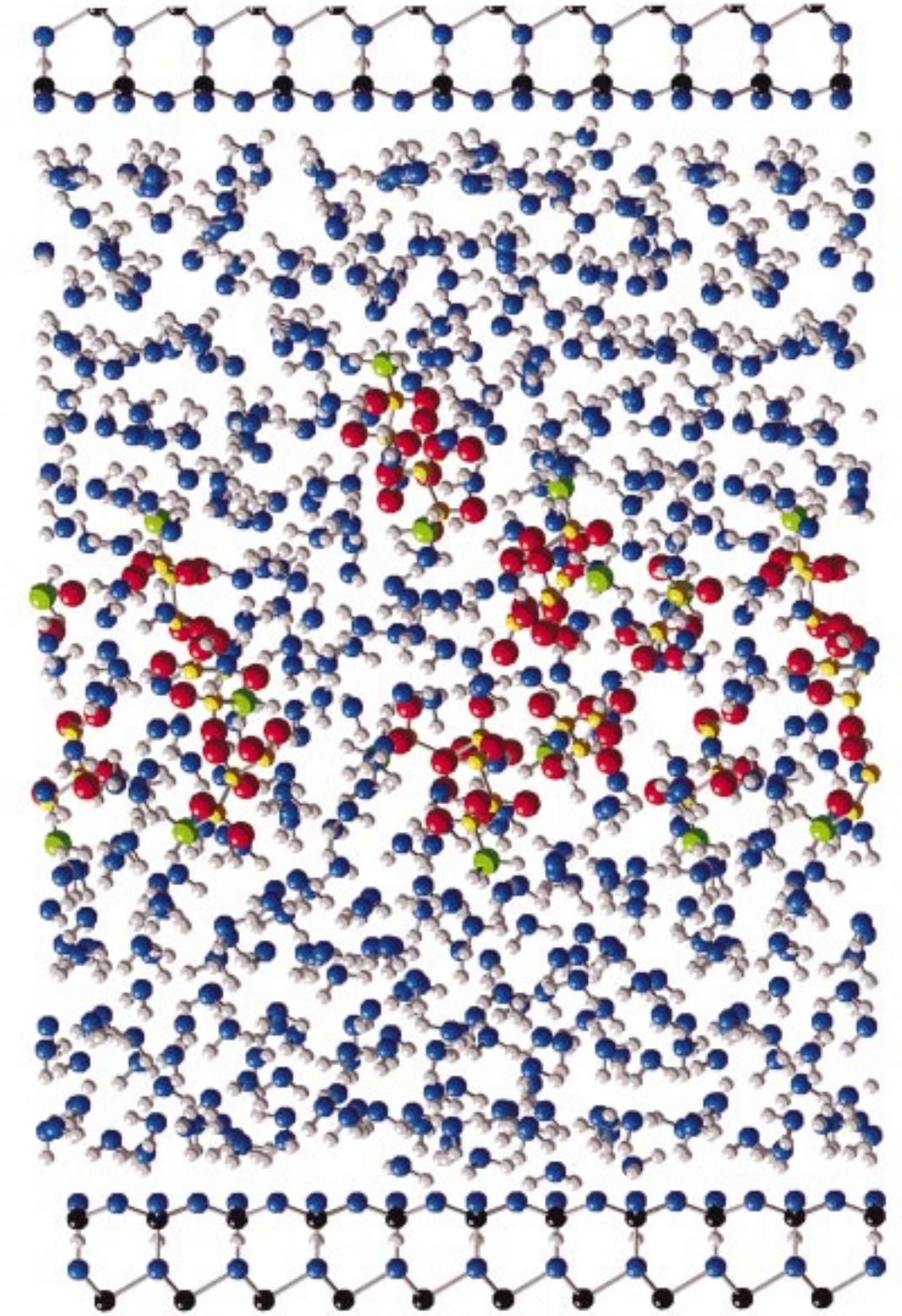

Figure 3. Molecular graphics snapshot of 12 unit cells of a 43.6 Å propylammonium vermiculite gel, illustrating how the majority of the counterions are separated from the charged clay surfaces by two layers of partially orientated water molecules. Atoms are color-coded: labelled hydrogen/deuterium (red); oxygen (blue); hydrogen (white); carbon (yellow); nitrogen (green); silicon, magnesium, aluminum (black).

Current understanding of the electrical double layer is based largely on theoretical studies of primitive model systems, in which the solvent is treated as a structureless dielectric continuum. In broad terms these studies identify two regions within the aqueous medium.[19] First there is the "Stern" layer of immobile counterions, attached to the solid surfaces. The ion concentration in this layer is treated as an empirical parameter. Second, there is a diffuse atmosphere of ions beyond the Stern layer. The properties of the diffuse ionic cloud are usually obtained by solution of the Poisson−Boltzmann equa-

tion.[8−10] The predicted counterion density is therefore at a maximum close to the solid surfaces, and at a minimum around the midplane.

Our results show that, in contrast to traditional models, the region within 6 Å of the clay surface consists principally of partially ordered layers of water molecules. This structural model of the interfacial water is, however, consistent with previous studies of hydrated surfaces, including surface X-ray scattering,[20] computer simulation,[21−24] surface force apparatus (SFA),[25] and neutron diffraction.[26] For example, SFA measurements of the interaction between two mica surfaces immersed in aqueous solutions show that at separations of less than 15 Å there is an oscillatory component to the surface−surface force. Typically, five force maxima are recorded with a period of 2.5 ± 0.3 Å.[25] Our current results suggest that these maxima in the surface−surface force can be attributed to the disruption of discrete layers of water molecules at the mica surfaces. Now that we have a detailed structural picture, SFA measurements on propylammonium vermiculite would provide an extremely useful aid to interpreting surface force data.

The counterion density in our system is found to be greatest around the center of the interlayer region, in direct opposition to the Poisson−Boltzmann distribution of primitive treatments. Furthermore, oscillations occur in the counterion density owing to the discrete nature of the ions, a factor that is not taken into account in the primitive model. We maintain that propylammonium ions can be considered ideal at this temperature and concentration. However, it is possible that the effective thickness of the (hydrated) clay surface precludes a diffuse counterion distribution when the clay layer spacing is 43.6 Å. Further experiments are therefore planned, using a layer spacing of around 50 Å (the maximum accessible to LAD). This will allow us to track the counterion and water distribution as the clay layer spacing is increased.

Conclusion

In this paper we present the first detailed structural measurement of the aqueous structure developed in the electrical double layer of a colloidal clay system. Our results show that, because of the favorable interaction of water molecules with surface charge sites, the majority of the counterions are separated from the clay surface by two partially ordered layers of water molecules. While contrary to traditional models, this result is consistent with previous experimental data and is analogous to the formation of hydration shells around simple ions in solution.[27] Our results illustrate that the molecular nature of the solvent plays a dominant role in determining the electrical double layer structure close to the surface. We find no conclusive evidence, however, of surface-induced structuring of the solvent extending much beyond two molecular diameters from the surface.

References and Notes

(1) Israelachvili, J. N. *Intermolecular and Surface Forces*; Academic Press: London, 1992.
(2) Hunter, R. J. *Foundations of Colloid Science I + II*; Clarendon Press: Oxford, 1986.
(3) Lipowski, J.; Ross, P. N. *Structure of Electrified Interfaces*; VCH: New York, 1993.
(4) Israelachvili, J.; Wennerström, H. *Nature* **1996**, *379*, 219.
(5) Newman, A. C. D. *Chemistry of Clays and Clay Minerals*; Mineralogical Society: London, 1987.
(6) Walker, G. F. *Nature* **1960**, *187*, 312.
(7) Braganza, L. F.; Crawford, R. J.; Smalley, M. V.; Thomas R. K. *Prog. Colloid Polym. Sci.* **1990**, *81*, 232.
(8) Williams, G. D.; Skipper, N. T.; Smalley, M. V.; Soper, A. K.; King, S. M. *Faraday Discuss.* **1996**, *104*, 295.
(9) Verwey, E. J. W.; Overbeek, J. Th. G. *Theory of Stability of Lyophobic Colloids*; Elsevier: Amsterdam, 1948.
(10) Van Olphen, H. *An Introduction to Clay Colloid Chemistry*; Interscience Publishers: New York, 1963.
(11) Sogami, I.; Ise, N. J. *Chem. Phys.* **1984**, *81*, 6320.
(12) Norrish, K. *Discuss. Faraday Soc.* **1954**, *18*, 120.
(13) Walker, G. F.; Milne, A. *Trans. 4th Int. Congr. Soil Sci.* **1950**, *2*, 62.
(14) Jinnai, H.; Smalley, M. V.; Hashimoto, T.; Koizumi, S. *Langmuir* **1996**, *12*, 1199.
(15) Soper, A. K.; Howells, W. S.; Hannon, A. C. *Analysis of Time-of-Flight Data from Liquid and Amorphous Samples*; CLRC Publications: Rutherford-Appleton Laboratory: Didcot, 1989.
(16) Skipper, N. T.; Soper, A. K., McConnell, J. D. C. *J. Chem. Phys.* **1991**, *94*, 5751.
(17) Desnoyers, J. E.; Arel, M. *Can. J. Chem.* **1967**, *45*, 359.
(18) Vennemann, T. W.; O′Niel, J. R. *Geochim. Cosmochim. Acta* **1996**, *60*, 2437.
(19) Stern, O. *Z. Elektrochem.* **1924**, *30*, 508.
(20) Toney, M. F.; Howard, J. N.; Richer, J.; Borges, G. L.; Gordon, J. G.; Melroy, O. R.; Wiesler, D. G.; Yee, D.; Sorensen L. B. *Surf. Sci.* **1995**, *335*, 326.
(21) Spohr, E. *Chem. Phys. Lett.* **1993**, *207*, 214.
(22) Rose, D. A.; Benjamin, I. *J. Chem. Phys.* **1993**, *98*, 2283.
(23) Xia, X.; Perera, L.; Essmann, U.; Berkowitz M. L. *Surf. Sci.* **1995**, *335*, 401.
(24) Delville, A. *Langmuir* **1992**, *8*, 1796.
(25) Israelachvili J. N.; Pashley, R. M. *Nature* **1983**, 306, 249.
(26) Swenson, J.; Smalley, M. V.; Thomas, R. K.; Crawford, R. J.; Braganza, L. F. *Langmuir* **1997**, *13*, 6654.
(27) Marcus Y. *Chem. Rev.* **1988**, *88*, 1475.